



Electrostatic Interactions to Attach Latex to Pigment Surface to Reduce Binder Migration

Pradnya D. Rao^{1,2}, Douglas W. Bousfield¹ and Carl P. Tripp^{1,2,*}

¹*Paper Surface Science Program, Department of Chemical and Biomedical Engineering, University of Maine, Orono, ME 04469, USA*

²*Department of Chemistry, Frontier Institute of Research in Sensor Technologies (FIRST), University of Maine Orono, ME 04469, USA*

Abstract: For many paints, paper coatings, and other pigmented coatings, latex and soluble binders are used to impart mechanical properties. However, non-uniform latex binder distributions are often observed in the thickness direction during application and drying, leading to quality issues. While several publications have documented this issue, few solutions are offered in the literature. Here we report a simple process to use electrostatic interactions to attach latex binder to pigments. Coating suspensions are generated using cationic precipitated calcium carbonate (PCC) pigments that are mixed with anionic styrene-butadiene (SB) latex binders resulting in latex-covered pigments. The migration of latex binder in coatings generated on various substrates under various drying conditions was measured using Raman spectroscopy and compared with reference coatings. The new system shows reduced latex binder migration for most situations than those obtained with the reference coating. The coated papers were also measured for strength, opacity, gloss, water drainage rate, and porosity. Little difference is seen in the picking strength of the coating and gloss compared to coatings prepared with standard formulations. Water drainage rate, opacity, and porosity were higher for latex-covered pigment (LCP) coatings than the reference standard coating; this increased porosity is likely due to the strong electrostatic attraction that exists between the cationic pigment and anionic latex binder that reduces the densification of the coating during drying.

Received on 31-12-2021
Accepted on 16-02-2022
Published on 11-05-2022

Keywords: Binder migration, cationic pigment, porosity, opacity, binder attachment, paper coating.

<https://doi.org/10.6000/2369-3355.2022.09.01>

1. INTRODUCTION

A latex binder is needed in water-based pigment suspensions to obtain durable coatings in a wide range of applications, such as lithium-ion batteries [1,2], paints [3,4], and paper coatings [5,6]. For all systems, the pigments and binder are mixed in a suspension that is applied to a substrate and dried. This movement of the binder relative to the pigments may decrease the effectiveness of the binder, resulting in quality issues. In the ideal case, the binder ends up being uniform within the coating layer. However, during application and drying, the latex binder may, in some cases, either concentrate or deplete at the surface of the coating [7].

In paper coatings, the type and amount of the latex binder present in the coating formulations affect the structure and surface composition of coated paper: this influences key properties, such as print gloss, stiffness, roughness, ink

settling rate caused by absorption, and print mottle [8,9]. The migration of latex binder is of critical interest, either away from the surface due to absorption into the paper or towards the surface during drying. This migration can influence the final properties of the coating layer and the efficient use of the latex. Latex binder distribution and migration in paper coatings have been the subject of numerous studies [10-13]. Latex binder migration in the paper structure, depletion, or concentration at the surface, has been observed and depends on parameters such as base paper absorption rates, pigment size, and drying conditions [7,14].

Various analytical techniques have been used to study latex binder migration and the analysis of the coating surface [14]. Latex binder migration has been identified in paper coatings by ultra-violet absorption (UV) [15] and attenuated total reflection infrared absorption (ATR-IR) spectroscopy [16-18]. Raman spectroscopic methods have been used to characterize latex and starch levels relative to the pigment for a number of parameters [16,19,20]. Scanning electron microscopy (SEM) has been used to visualize latex

*Department of Chemistry, Frontier Institute of Research in Sensor Technologies (FIRST), University of Maine Orono, ME 04469, USA; E-mail: ctripp@maine.edu

concentrations after staining with OsO_4 as well as electron spectroscopy for chemical analysis (ESCA): recent work is summarized by a few different groups [21-23]. Recently, high-quality cross-section images of coated papers were obtained using field emission scanning electron microscopy in combination with an argon-ion-beam milling technique to study detailed positions of latex and pigment in the coating layer [24,25]. Latex is found to not only enrich the coating surface but can migrate internally in the coating layer from regions of large pores to fine pores. Atomic force microscopy (AFM) has also been used to measure the latex distribution in the presence of large-size pigments [26,27]. The latex was found to fill up the voids in the coating pigment. Laser-induced plasma spectroscopy (LIPS) has been used to study latex binder migration of starch and latex under intense air-drying conditions [28].

Several models have been proposed to explain the movement of the latex binder during the drying step. In the capillary transport model proposed by Hagan [29], as the water evaporates, the pigment particles move closer to form capillaries. These capillaries provide passage for the latex binder to be transported to the top surface with the movement of water molecules during evaporation. The absorption flow model discusses the motion of latex away from the surface as the water phase of the coating absorbs into the paper base [20]. A Brownian motion model was recently proposed where latex binder migration occurs during the initial drying stage [30,31]. The smaller latex particles exhibit higher Brownian motion relative to the larger pigments and migrate to the air-liquid interface, where they become trapped and lose their mobility. In this case, the surface is proposed to be latex rich even before the pigments come together to form capillaries and before any drying. In the boundary wall depletion model, the concentration of the smaller latex particles occurs at the top of the coating surface boundary because the small particles lubricate the coating blade boundary because of their size resulting in a high concentration of latex binder in

the wet coating layer [32-34]. While these various models explain some of the results, they are based on quite different physical phenomena. It is not clear in the literature what model best describes the situation. Also, some computer-based models describe the effect of substrate and latex binder diffusivity on the binder migration of the coated papers [35].

In paper production, cationic polymers or other retention aids are often used to help fine pigments and fibers adsorb on to large fibers to increase the retention of these fine fibers and pigments in the paper [36-40]. This suggests a similar technique could be used in the coating layer. This same concept could be used to reduce latex binder migration by attaching the fine latex particles to the pigment. Figure 1 shows the concept of taking a cationic pigment combining it with an anionic latex binder to produce a latex-covered pigment (LCP). This situation contrasts with the typical system where both the latex and pigment are anionic, also depicted in Figure 1. The cationic pigment may be produced by adsorbing cationic polymer or starches on the pigment or may occur naturally, as with precipitated calcium carbonates. The reverse is also possible, where cationic latex is exposed to anionic pigments, but the result of that would likely be a system that is overall cationic; cationic systems are difficult in many industrial processes. The expected result is that once the latex is adsorbed onto the pigment, it should not be able to move relative to the pigment during coating and drying.

Here, a method is attempted to form a cationic pigment particle coated with anionic latex binder particles in the wet state. By electrostatically attaching the latex binder to the pigment, an anionically stabilized suspension was generated that has the potential to decrease latex binder migration and improve paper properties. This study aims to investigate the potential of this approach to prevent or reduce latex binder migration and to report on the properties of these coatings. Anionic styrene-butadiene (SB) latex particles are added to cationic precipitated calcium carbonate (PCC) to form an

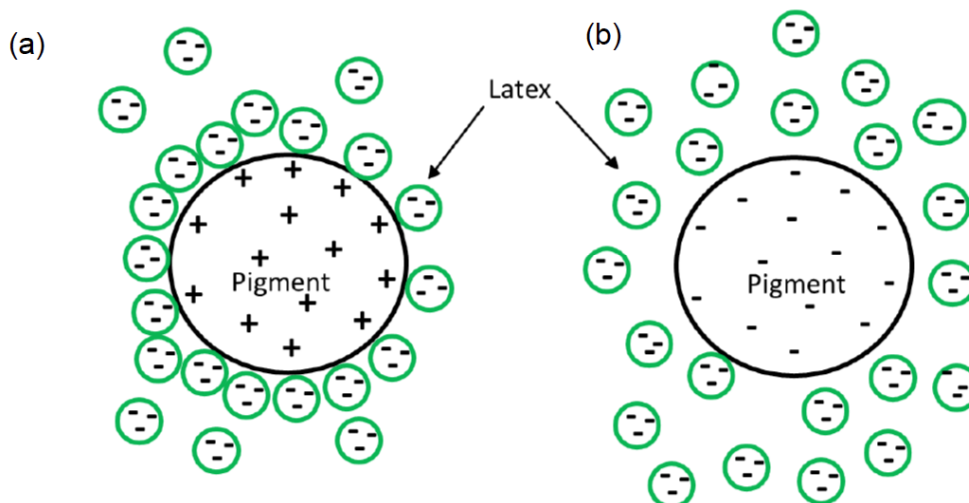


Figure 1: (a) Latex attached to a cationic pigment (b) typical coating system.

LCP, with the cationic PCC at the core surrounded by the SB. Raman spectroscopy was used to measure the ratio of SB latex to PCC at the surface of a coating layer applied onto the various substrates such as glass, paper, and blotter paper. The coatings' strength, opacity, gloss, water drainage, rheology, and porosity were also measured and compared to the standard anionic coating. To our knowledge, this is the first time that cationic PCC in the core is surrounded by anionic SB latex to create an overall anionic coating suspension. Traditional paper coatings contain pigments and latex binders that are anionically charged, and therefore, there are no electrostatic interactions between the pigments and latex binders. While various mechanisms have been proposed to explain binder migration, this has not translated to methods to reduce or prevent binder migration using electrostatic interactions. This is the unique aspect of our research presented in this paper. Furthermore, the method used to generate LCP is a very simple and industrially scalable process.

2. EXPERIMENTAL

2.1. Materials

PCC at 48% solids with a measured average particle size distribution of 1.5-3 μm and zeta potential of +32 mV was supplied by Minerals Technologies as a filter cake. The PCC did not contain any dispersant and is naturally cationic. The SB latex (GenFlo 5086) at 50% solids was supplied by OMNOVA and had a glass transition temperature of -5°C with a measured average particle size distribution of 120-140 nm and zeta potential of -35 mV. The Sodium polyacrylate solution (Mw 15,000) at 20% wt./vol in water was supplied by Sigma Aldrich.

2.2. Methods

2.2.1. Particle Size and Zeta Potential Measurements

The particle size and zeta potential of the cationic PCC and anionic SB latex binder were measured on a Malvern Zetasizer after a 100-fold dilution of the sample to obtain approximately a 0.5% solid content level. The cationic supernatant was collected and used to dilute 1 mg of cationic PCC cake to obtain a 100-fold dilution instead of DI water, to avoid a change in pH and calcium ion content after dilution. The cationic supernatant was obtained by centrifuging 100 g of cationic cake at 2200 RPM for 8 mins from the stock. A 1 mg sample of the SB latex binder was diluted 100-fold using DI water for the SB latex binder. A similar procedure was used for anionic PCC, LCP formulations, and standard formulations to measure zeta potential and particle size.

2.2.2. Formation of LCP and Standard Formulation

The LCP formulations were made by adding different amounts of a latex binder to the cationic PCC pigments. In the paper industry, the latex addition level is often reported in terms of a mass of binder per hundred parts of pigment (pph).

Values that span a wide range were used from 10 to 30 pph. A 30 g quantity of cationic PCC cake (wet basis) was dispersed in 3 ml of cationic supernatant while stirring. Then, the anionic SB latex binder was added all at once to the PCC suspension under constant stirring at 550 RPM using a propeller-type mixer for 20 mins. DI water was then added to obtain a solid content of 45%.

Standard anionic formulations were produced using the same cationic PCC particles for comparative purposes. In this case, anionic PCC particles were first generated by adding 2 ml of sodium polyacrylate at 20 % wt./vol in one shot to a suspension containing 30 gm of cationic PCC (wet basis) while stirring at 550 RPM using an overhead propeller for 5 minutes. Particle size and zeta potential of the anionic PCC particulates were measured by a 100-fold dilution of the suspension with DI water. Standard formulations containing varying amounts (10, 20, 30 pph) of anionic SB latex were prepared by mixing latex with the anionic pigment. A 30 g quantity of anionic PCC cake (wet basis) was dispersed in 3 ml of DI water while stirring. The anionic SB latex binder was added to the anionic PCC under constant stirring at 550 RPM using a propeller-type mixer for 20 mins. The solid content of the final formulation was adjusted to 45% solids to be equivalent to LCP formulations. The viscosity of the LCP and standard suspension at 45% solid content was measured using a concentric cylinder device (Hercules Hi-shear).

For LCP formulations, samples were centrifuged to determine the amount of latex binder electrostatically bound to the underlying cationic PCC. The formulations with varying amounts of 10, 20, 30 (pph) of the latex binder were centrifuged at 2200 RPM for 8 mins. to separate solids from the liquid in the suspensions. The water phase and centrifuged cake were analyzed separately to determine the excess (unbound) latex content. The water phase was examined visually for turbidity. A small amount of centrifuged cake was analyzed in Raman spectroscopy. PCC and SB bands appeared at 1086 and 1001 cm^{-1} , respectively, and the SB/PCC band ratios were measured and converted to mass ratios using a calibration curve. A calibration curve was generated using standard formulations and LCP formulations at different amounts (5, 10, 30, 50 pph) of anionic SB latex. Raman spectra of each formulation were collected on stirred vials with the laser beam focused on the midpoint of the side of the vial. The calibration curve passed through zero for the LCP and standard formulations.

2.2.3. Coating

Coatings were made on three types of substrates: 1) blotter paper, a porous and highly absorbent substrate, 2) porous paper, with a basis weight of 50 g/m^2 and medium absorbent type, and 3) glass, a non-absorbent substrate. A lab rod drawdown coater was used for the paper substrates. Handmade coatings were made on the glass slides by depositing 1.5 ml of the suspension onto one end of the glass slide and then using a spatula to drag down the deposited suspension to the other end of the glass slide. The estimated

coat weights on the glass slides were in the range of 13 ± 2 g/m², and the measured coat weight on the paper and blotter paper were in the range of 12 ± 2 g/m².

2.2.4. Raman Spectroscopy

Raman spectroscopy was used to analyze the surface composition of the coatings, as well as the base paper sheets. For both standard and LCP formulations, four paper coatings were made for each formulation. Each paper coating was analyzed at three different positions. For each formulation, the average value of the total of 12 readings was reported.

Raman spectra were collected using a Renishaw Raman 1000 imaging microscope system. The excitation source is an SDL-XC 30 diode laser from SDL Inc, operating at a wavelength of 785 nm and 35 mW power. The spot size was approximately 2 mm in diameter with a 4 μm penetration depth using a 5X LEICA N PLAN objective [21]. Coated papers were cut into 2x2 cm² pieces. PCC and SB bands appeared at 1086 and 1001 cm⁻¹, respectively, and the SB/PCC band ratios were measured and converted to mass ratios using a calibration curve. Raman analysis of the base paper did not show any bands of PCC or SB. For each sample, integration time was 10 secs, and 4 scans were recorded for each spectrum. SB/PCC band ratios were determined for two sets of coated samples, one set dried at room temperature overnight (16 h.) and another set dried at 105°C in an oven for 4 mins.

2.2.5. IGT Pick Test

The IGT pick test device evaluated the coating strength using the standard method TAPPI T514. The instrument was set to an accelerated mode with a final pick velocity of 4 m/s. A medium viscosity (52 Pa. s) ink was used to perform the IGT pick test. In this test, a viscous ink that simulates a printing ink is printed onto the coated paper in an accelerating manner: the velocity where the coating layer delaminates is the pick velocity.

2.2.6. Gloss

A gloss of the coated paper was measured using standard method TAPPI T480 using a Glossmeter manufactured by Technidyne Corporation. The Glossmeter was calibrated using gloss standard 96.1. For each sample, 10 readings were taken at different spots, and the average value is reported.

2.2.7. Opacity

The opacity of papers coated using LCP formulations was measured with TAPPI standard method T519 using a Color TouchX device manufactured by Technidyne Corporation. The references used for the opacity experiments were recorded using a stack of 3 sheets of coated papers. This type of opacity measurement is known as the "opacity by paper backing". Three sheets of coated papers were used in the backing experiment to obtain a reading of $R_{\infty} = 100\%$.

Hence it was sufficient to use a stack of three coated papers as a reference in the opacity measurements.

2.2.8. Porosity

The porosity of the coatings was measured using a silicone oil test. Coatings were made on the plastic (non-porous substrate) and dried overnight. Coated samples were cut into pieces of 2x2 cm² and measured for thickness and weight. Then all samples were covered in silicone oil for 45 mins. The excess oil on the surface was removed with wipes, and the sample was weighed. The porosity of the coating was calculated as

$$e = (W_o - W_d) / \rho_o AL \quad (1)$$

Where W_o is the weight of oil-saturated coating on plastic, W_d is the weight of dry coating on plastic, ρ_o is the density of the silicon oil, A is the sample's surface area, and L is the thickness of the sample.

2.2.5. Water Drainage

The rate of water drainage from the coating was determined using the standard method TAPPI T701 using an Abo Akademi Gravimetric Water Retention (AA-GWR) instrument. The water drainage rate was calculated at 30 secs under a pressure of 1 atmosphere. The coating is separated from an absorbent blotter paper by a membrane. The weight gain of the paper measures the amount of water drained from the coating.

3. RESULTS AND DISCUSSION

3.1. Zeta Potential and Particle Size

The zeta potential and average particle size distribution of the cationic PCC were +32 mV and 1.5-3 μm, respectively. The corresponding values for the anionic SB latex binder were -35 mV and 120-140 nm, respectively. The zeta potential of the LCP was -30 mV, showing that the cationic PCC was converted to anionic with a layer of SB latex binder. Furthermore, the average particle size of the LCP increased to 2.5-4 μm: this increase also indicates that the addition of the SB latex to the cationic PCC did not lead to an aggregated structure but rather to a layer of SB lattices surrounding each PCC particulate. In the control experiments, the aim was to convert the cationic PCC to an anionic PCC without changing the size of the particle. The average size of the anionic PCC was 1.5 to 3 μm. This is the same size distribution as the cationic PCC cake. However, the zeta potential of anionic PCC was -20 mV. The LCP particles are 0.4-1 μm larger than the cationic and anionic pigments. Therefore, coatings of LCP did not show any difference in the coating caliper when compared to coatings of the standard formulation.

3.2. Adsorption of SB Latex on Cationic PCC

When the LCP suspensions were centrifuged, the 10 and 15 pph latex binder supernatants were clear whereas, the

supernatants were cloudy for the standard formulations. For 20 pph and higher latex binder levels, a turbid supernatant layer was collected for cationic pigments. Raman spectral analysis of the supernatant showed only the presence of latex binder. Thus, about 15 pph latex binder was found to be attached to the cationic pigment surface. This value was further confirmed by Raman analysis of the centrifuged cake of the LCP formulations. For 10 and 15 pph formulations, the Raman spectra showed that the relative amount of pigment to latex binder in the cake was equal to the amounts used to prepare the formulation whereas, for 20, 30, and 50 pph, 17, 19, and 25 pph latex binder, respectively, were measured in the centrifuged filter cake. This result confirms that for 20 pph and higher, there is a free latex binder in the system. Centrifuging the anionic coatings at any concentrations from 20 pph results in a cloudy supernatant.

A maximum loading of 15 pph latex binder for the LCP is consistent with the values obtained using the following simple calculation. The total volume of an LCP sphere was calculated using a radius equal to the PCC radius plus the diameter of the latex binder, assuming full coverage of the PCC surface with a latex layer. The volume ratio of latex to pigment would be the volume of the total sphere minus the pigment volume divided by the pigment volume. This volume ratio is converted to mass ratio using the densities of latex and pigment. For any radius of latex and pigment, R_L and R_p , respectively, the mass ratio of latex to pigment based on these volumes is given by

$$M_V = \left(\frac{(R_p + 2R_L)^3}{R_p^3} - 1 \right) \frac{\rho_L}{\rho_p} \quad (2)$$

Where ρ_L and ρ_p are the densities of the latex and pigment, respectively.

If this mass ratio is calculated based on the surface area, where the latex covers a projected area on the surface of the pigment, an expression can be developed that gives the mass ratio based on the surface area as

$$M_{SA} = \frac{4R_L\rho_L}{R_p\rho_p} \quad (3)$$

The expression based on surface area coverage includes the influence of voids between latex particles. Figure 2 compares these expressions. For the smallest pigment size of the range measured (1.5 μm) and the latex size (120 nm), the latex to pigment size ratio is 0.08. This 0.08 ratio correlates to 13 to 22 pph for M_{SA} and M_V , respectively. This agrees with the experimental results of 15 pph of latex binder attached to the surface of cationic PCC.

3.3. Rheology

The suspensions with LCP had higher viscosities than suspensions of the standard system. Figure 3 shows the viscosity-shear rate results for 10, 20, and 30 pph

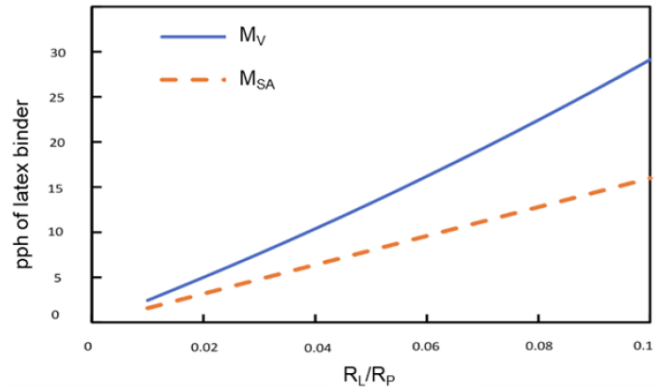


Figure 2: Dependence of particle size ratio on the amount of SB latex required to cover one pigment particle based on volume concept (M_V) and surface area (M_{SA}).

formulations for the LCP and the standard formulations. As the latex content increases, the viscosities decrease for all systems; free latex binder in the system must help break up structures and allow for easy motion of pigments under shear. The LCP, as depicted in Figure 1, would be bulkier or take up more volume because water is trapped between the latex at the pigment surface. Cationic and anionic interaction leads to an increase in the overall viscosity, which is consistent with the literature [41]. At solids higher than 45%, the LCP formulations had viscosities that were too high to measure with the equipment available, but the standard formulation has viscosities of 20-25 cP even at 60% solids. Therefore, a key drawback of using the LCP is the rheology of these systems above 45% solids. All suspensions were used at 45% solid content to be consistent, even though this level is lower than that typically used in the industry. At 45% solids, there could be more latex binder migration compared to the 60% or higher solids used in practice. However, the purpose of this work was to investigate the concept of using a central cationic PCC pigment with a layer of the electrostatically bound latex binder as a means for lowering latex binder migration, rather than to generate high solid formulations.

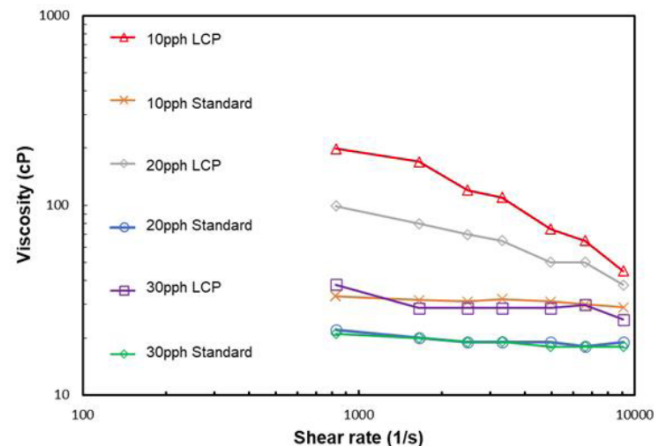


Figure 3: Shear rate vs. viscosity of standard and LCP coating formulations at 45% solids.

3.4. Raman Spectroscopy

Figure 4 shows the Raman spectra obtained for the various SB/PCC coatings used in this study. Two peaks are observed at 1086 and 1001 cm^{-1} . The band at 1086 cm^{-1} is the C-O stretching mode in the PCC peak, and the band at 1001 cm^{-1} is the ring breathing mode of SB. Since the laser beam's penetration depth is about 4 μm into the coating, a change in the relative intensity of these two Raman bands is due to a change in the relative amount of the PCC to SB in the top 4 μm region of the coating. Others have demonstrated that there was no difference in SB/PCC ratio for thinner (8-10 μm) vs. thicker (18-20 μm) coating in the same region.

In conclusion, it is mentioned that paper coatings are very dispersive. The roughness of coated paper does not affect the results of the ratio of surface concentration of SB/PCC obtained using Raman spectroscopy [21]. In our experiment, a baseline correction was performed to determine the binder migration first. The peak heights of the SB and PCC bands were measured using a valley-to-valley baseline correction, and the ratio of SB/PCC was determined. As seen in Figure 4, the LCP coatings have a lower SB/PCC band ratio than their corresponding coatings generated using the same weight of binder in the standard formulation. This shows that LCP formulations have less SB binder present on the surface than coatings produced using a standard formulation. Similar trends were observed for coatings dried in the oven at 105 $^{\circ}\text{C}$.

Figure 5 shows the Raman SB/PCC band ratios obtained for standard and LCP formulations at different latex binder levels and on all three substrates. For all formulations, the SB/PCC band ratios exceed the values obtained for the bulk suspensions shown as the calibration curve: these results show that latex binder enrichment of the surface occurs in all cases and on all substrates because the Raman signal is from the top 4 μm of the coating layer [21]. This enrichment is a surprise on the absorbent substrates that quickly pull the water phase from the coating into the blotter paper; this movement of water should drag the latex binder layer away

from the top surface. However, latex binder enrichment is reported in several papers [32,33], and it is explained by early models such as Hagen [10], where capillaries formed in the coating layer that creates a flow of liquid towards the surface during drying that allows latex binder particles to migrate to the surface. Pan *et al.* [35] and Scriven *et al.* [42] proposed models that showed the difference between the latex binder distribution of porous substrates such as paper and non-porous substrates, like a glass slide. Porous substrates tend to deposit more latex binder on the surface than the non-porous substrates because of air invasion of the paper allows for flow towards the surface. During drying of a porous substrate like paper, coatings have heavy latex binder deposits in the top layer as liquid moves towards the surface during the drying event. In the case of non-porous materials, liquid resides longer in the lower layer and deposits more latex binder in the lower pores and less on the coating surface [35, 42]. This explains that paper has more latex binder on the surface than glass slides.

The LCP formulations had significantly less latex binder enrichment for the glass slide and the regular paper than the standard formulation. This result follows the hypothesis for the work in that attached latex will not be able to move during drying stages. For the paper sample, the latex content at the surface is near the formulation within the standard error. The glass results are quite similar to the paper. For the standard formulation, the paper results have a surface latex content that is 50% greater than the bulk composition; significant motion of latex to the surface during drying occurs. On the glass, the enrichment is around 35%.

The results on the blotter paper are surprising in that the enrichment with the LCP formulations is more than what is seen with the standard formulation. For the standard formulation, all the latex particles are free to move, and it is expected that latex is pulled rapidly into the pore structure of the paper with the water and gets trapped in the blotter paper, thus is not able to enrich at the surface during drying which could deplete the coating layer of latex for the standard

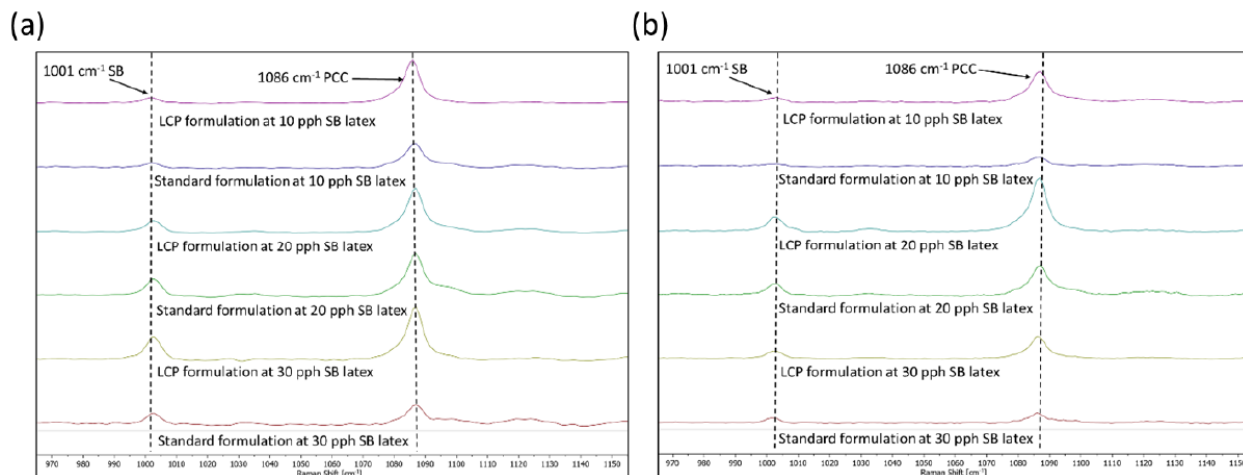


Figure 4: (a) Raman spectra of air-dried paper coatings (b) heat-dried paper coatings.

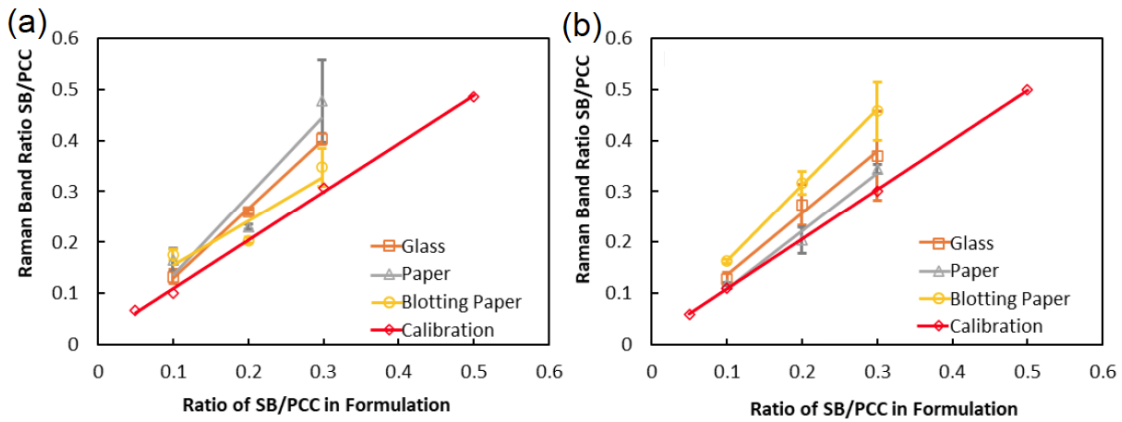


Figure 5: SB/PCC band ratio of (a) standard formulations (b) LCP formulations at 10, 20, and 30 pph latex binder dried at room temperature.

formulation. The blotter paper is quite absorptive, and during coating, the liquid phase is pulled away from the coating layer into the blotter paper.

Also, in the standard formulation, large pigment particles are trapped at the surface of the paper and form a dense filter cake. This action leads to heavy pigment deposits and potential bridging at the surface of the blotter paper that blocks latex binder particles from moving back towards the coating surface, resulting in latex binder particles being stuck in the bottom part of the coating layer. This phenomenon is also called as size exclusion effect. These mechanisms can explain why the standard formulation coatings on blotter paper have less latex binder on the surface than the LCP formulations.

However, in the case of LCP coating on blotter paper, latex has shown lower mobility as 15 pph latex is attached to the pigment surface. Also, on blotter paper, drying is relatively slow as water tends to reside in the pores for a longer time. In such cases, when the latex binder mobility and drying rate are slow, more latex binders tend to deposit on the surface of the coating because this type of system has a high Peclet number around 10^3 explained by the pore level model [36].

Also, for the LCP formulation, particle size is slightly larger than the standard formulation due to an additional layer of SB latex on the cationic PCC surface; thus, the latex is retained in the coating layer, and during drying, can migrate the small distance to the surface. This is similar to what LePoutre [43] found that coarser PCC particles form bigger voids in the coating structure on highly absorbent paper. This mechanism explains that LCP showed more latex binder on the coating surface than the standard formulation when coated on the blotter paper.

Figure 6 shows the results for rapidly drying samples in an oven compared to air drying. Heat dried standard formulation on paper showed the highest latex binder enrichment among all coatings using LCP and standard formulations. This is consistent with the literature that reports increased drying temperature links with latex binder enrichment on the 70 g/m^2 base paper [44,45]. For all LCP formulations, drying at 105°C showed slightly higher latex binder migration than air-drying glass and paper substrate samples. This could be attributed to the fact that 15 pph of the SB latex binder is attached to the cationic PCC surface and not moving during the coating process and consolidation. However, the remaining latex

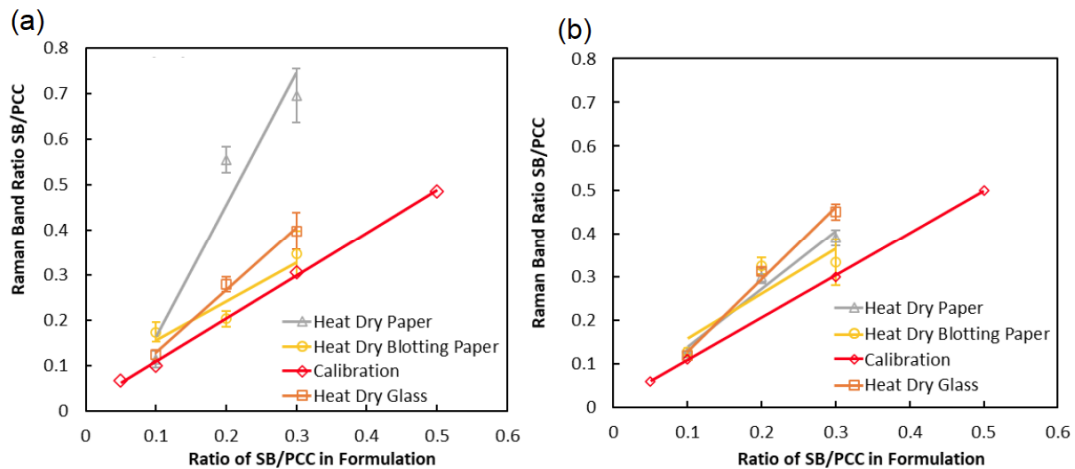


Figure 6: SB/PCC band ratios were obtained for coatings using (a) standard formulations (b) LCP formulations at 10, 20, and 30 pph of latex binder dried at 105°C .

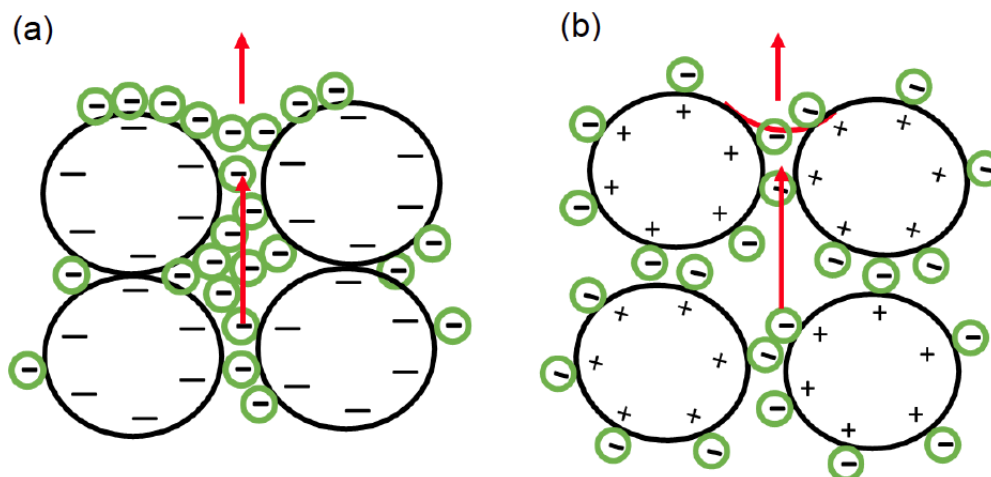


Figure 7: Schematic of latex binder migration towards the surface during the evaporation near the surface with (a) latex binder particles free to move (b) latex binder attached to the pigment surface.

binder is free to move, and increasing with temperature may have accelerated the latex binder particle movement to the surface of the coating layer, which resulted in more latex binder on the surface.

However, on blotter paper, air drying conditions showed higher migration than that of the heat dry conditions for formulations. This result could be caused by the time scale for the free latex binder to migrate towards the surface. Absorption on the blotter paper pulls the free latex binder from the surface, but if the surface layer pores empty due to rapid drying at a higher temperature, the latex binder is not able to reach the pores due to faster immobilization at higher temperature and pores empty deeper into the structure [35]. Therefore, a possible explanation is that the high-temperature drying can empty the surface pores more rapidly than capillary flow to the pores, and this causes faster immobilization of the binder particles, resulting in little enrichment at the surface.

Overall, formulations with the LCP showed less latex binder migration than that of standard formulations on the air and heat-dried paper and air-dried glass slides. The almost same amount of latex binder migration was observed in standard and LCP formulation at oven-dried conditions on a glass substrate. However, in the blotter paper case, SB latex binder particles got trapped in the blotter paper for the standard

formulation. They can enrich the surface in LCP formulation because bigger voids are formed in the LCP formulations in air-drying conditions.

When the drying of a coating layer occurs, capillaries form near the surface of the coating. If the capillary is stable, the latex binder will migrate to the surface as water flows to fill these pores and evaporates from the surface [4,5]. Suppose a latex binder is attached to the pigment through electrostatic interactions. In that case, it has less chance to move towards the surface to enrich the surface or deplete the paper's bottom layers. Figure 7 depicts this situation. Suppose a latex binder is first pulled away from the surface due to water absorption into a porous structure like paper. In that case, the latex binder can still move back towards the surface because the fine pores generate stable capillaries.

3.5 Coating Strength, Porosity, Opacity, and Water Drainage

The physical properties of the coating layers are reported in Table 1 for the coatings applied on the paper. There was no significant difference observed in the pick strength values of the papers coated with the LCP, even though latex binder enrichment at the surface was reduced. A possible reason could be that the latex binder in the LCP formulations cannot move locally to pigment-pigment contacts during drying. Due to the lack of the freedom of SB latex particles to move,

Table 1: Properties of coatings made using standard and LCP formulations.

Properties	10pph		20pph		30pph	
	Standard	LCP	Standard	LCP	Standard	LCP
IGT test-Pick Velocity (m/s)	1.2 ± 0.1	1 ± 0.1	1.6 ± 0.3	1.2 ± 0.3	3.4 ± 0.1	3 ± 0.1
Porosity	10%	15%	1-2%	5%	<1%	1-3.5%
Opacity	90 ± 0.4	93 ± 0.5	89.6 ± 0.3	92 ± 0.1	89 ± 0.4	90 ± 0.1
Gloss	8 ± 0.2	6.6 ± 0.2	8.3 ± 0.1	8.2 ± 0.1	8.5 ± 0.1	8.3 ± 0.1
AAGWR (g/m ²)	47 ± 11	348 ± 10	29 ± 7	719 ± 48	14 ± 7	746 ± 17

consolidation of the coatings was hindered as well as the film formation of the latex, which may result in no improvement in the picking strength. Calendaring was performed at 120 °C in the initial trials of coatings of LCP. However, there was no difference observed in the picking strength. Also, no cracks were observed in the coating layer.

The 10, 20, and 30 pph LCP formulations showed higher water draining rates when compared to the corresponding standard coating formulations (see Table 1). This is consistent with the porosity measurements that show that LCP has a more open and porous structure as the pigments pack into a filter cake. This open structure allows for a higher water flow, thereby increasing the AAGWR values. A lower amount of free latex in the system leads to an increase in the pore space, as shown by the porosity values given in Table 1.

The 10 pph LCP formulations showed the highest porosity among all the samples reported in Table 1. Overall, LCP formulations at 10 and 20 pph showed a 5% increase in porosity than values obtained for standard formulations at 10 and 20 pph. This is attributed to the larger voids in the coating structures because the latex binder is adsorbed on the pigment and can no longer move to fill the void structure during coating consolidation. In contrast, no significant difference was observed in the porosity of coatings for LCP and standard formulations at the 30 pph latex binder content. As calculated and shown by centrifugation results, the 30 pph LCP has 11pph free latex present in the formulation. Thus, the free latex in 30 pph LCP and standard formulations fill the pores, resulting in a similar porosity.

The higher porosity of LCP coatings is also responsible for the improved opacity of these coatings. Opacity data for 10, 20, and 30 pph LCP's and standard formulations are also shown in Table 1. In all cases, coatings made using LCP formulations showed higher opacity than standard formulations. These results further reinforce that the coatings with the LCP are more porous than that of the coatings made using a standard formulation, and the open structure causes reflected light to scatter in all directions to increase opacity.

Coatings produced using the standard formulation at 10 pph latex binder showed a higher gloss than those obtained with 10 pph LCP formulations. At 10 pph, the standard formulation has a free latex binder enriched at the surface and fills the voids leading to a glossy surface. In the 10 pph LCP, there is no free latex binder to fill the voids at the surface, leading to a lower gloss value. This further confirms that LCP formulation at 10 pph can reduce binder migration when compared to a standard formulation at the same latex binder concentration. Both 20 and 30 pph LCP formulations have 3 and 11 pph free latex binders to fill the voids at the surface, respectively, resulting in the same gloss as those obtained using standard formulations at 20 and 30 pph latex binders.

4. CONCLUSIONS

SB latex was attached to cationic PCC particles simply using electrostatic interactions to generate an LCP. A maximum of

about 15 pph of the latex was determined to be attached to the pigments used in this study. The viscosity of these LCP formulations was higher than the standard formulations at all latex contents and increased to levels too high to coat when the solids are over 45%. Latex binder migration was reduced concerning standard formulations for all conditions, except for coatings on the blotter paper dried at air temperature. This result on blotter paper may be caused by how the latex binder moves into the sheet during the application. The latex binder gets trapped away from the top coating surface for the standard formulation. The LCP formulations had an increased opacity, porosity, and dewatering rate compared to the standard formulations; these results indicate a more porous coating layer for the LCP formulations than the standard.

ACKNOWLEDGMENTS

We would like to thank the University of Maine Paper Surface Science Program and the industrial sponsors for their support of this work.

REFERENCES

- [1] Hitomi S, Kubota K, Horiba T, Hida K, Matsuyama T, Oji H, Yasuno S, Komaba S. Application of acrylic-rubber-based latex binder to high-voltage spinel electrodes of lithium-ion batteries. *ChemElectroChem* 2019; 6: 5070-5079. <https://doi.org/10.1002/celec.201901227>
- [2] Isozumi H, Horiba T, Kubota K, Hida K, Matsuyama T, Yasuno S, Komaba S. Application of modified styrene-butadiene-rubber-based latex binder to high-voltage operating LiCoO₂ composite electrodes for lithium-ion batteries. *J Power Sources* 2020; 468: 228332. <https://doi.org/10.1016/j.jpowsour.2020.228332>
- [3] Danková M, Kalendová A, Machotová J. Waterborne coatings based on acrylic latex containing nanostructured ZnO as an active additive. *J Coatings Technol Res* 2020; 17: 517-529. <https://doi.org/10.1007/s11998-019-00302-6>
- [4] Worlee A, Homdong N, Hayemasae N. Application of polymer blend based on natural rubber latex and acrylic resin as a binder for wall paints. *IOP Conference Series: Materials Science and Engineering* 2020; 773: 12-32.
- [5] Kwon S, Oh K, Shin SJ, Lee H.L. Effects of hydroxyethyl methacrylate comonomer in styrene/acrylate latex on coating structure and printability. *Prog Org Coatings* 2020; 147. <https://doi.org/10.1016/j.porgcoat.2020.105862>
- [6] Kwon S, Oh K, Shin SJ, Lee HL. Structural changes of the coating layer by styrene/acrylate latex with hydroxyethyl methacrylate. *ACS Omega* 2019; 4: 18405-18412. <https://doi.org/10.1021/acsomega.9b02671>
- [7] Al-Turaif HA, Bousfield DW. The influence of pigment size distribution and morphology on coating binder migration. *Nord Pulp Pap Res J* 2005; 20: 335-339. <https://doi.org/10.3183/nppri-2005-20-03-p335-339>
- [8] Lepoutre P. The Structure of paper coatings: An update. *Prog Org Coatings* 1989; 17: 89-106. [https://doi.org/10.1016/0033-0655\(89\)80016-0](https://doi.org/10.1016/0033-0655(89)80016-0)
- [9] Lee HL, Youn HJ, He M, Chen J. Back-trap mottle: A review of mechanisms and possible solutions. *BioResources* 2021; 16: 6426-6447. <https://doi.org/10.15376/BIORES.16.3.LEE>
- [10] Hagen KG. Fundamental assessment of the effect of drying on coating quality. *TAPPI Coat Conf* 1985; 69: 131-137.
- [11] Du Y, Liu J, Wang J, Wang B, Li H, Su Y. Starch-based bio-latex redistribution during paper coating consolidation. *Prog Org Coatings* 2017; 106: 155-162. <https://doi.org/10.1016/j.porgcoat.2017.02.016>
- [12] Nechita P. The influence of drying conditions of clay-based polymer coatings on coated paper properties. *Coatings* 2021; 11: 1-13. <https://doi.org/10.3390/coatings11010012>

- [13] Kline JE. Fundamental aspects of latex mobility in paper coatings. Tappi Advanced Coating Fundamentals Symposium Proceedings; 1993; 93-100.
- [14] Groves R, Matthews GP, Heap J, McInnes MD, Penson JE, Ridgway CJ, C.F.Baker. Binder migration in paper coatings - a new perspective. 12th Fundamental Research Symposium 2001; 1149-1182.
- [15] Fujiwara H, Kline JE. Ultraviolet absorption of styrene-butadiene latex on pigment-coated paper. Tappi Journal 1987; 70: 97-100.
- [16] Kenttä E, Pöhler T, Juvonen K. Latex uniformity in the coating layer of paper. Nord Pulp Pap Res J 2006; 21: 665-669. <https://doi.org/10.3183/nppri-2006-21-05-p665-669>
- [17] Chattopadhyay R. Dynamics of particle movements in paper coatings. Ph.D. thesis. University of Maine 2014.
- [18] Halttunen M, Löija M, Vuorinen T, Stenius P, Tenhunen J, Kenttä E. Determination of SB-latex distribution at paper coating surfaces with FTIR/ATR spectroscopy. Tappi Coating and Graphic Arts Conference and Trade Fair; 2003; 203-211.
- [19] He P, Bitla S, Bousfield D, Tripp CP. Raman spectroscopic analysis of paper coatings. Appl Spectrosc 2002; 56: 1115-1121. <https://doi.org/10.1366/000370202760295322>
- [20] Bitla S, Tripp CP, Bousfield DW. A Raman spectroscopic study of migration in paper coatings. J Pulp Pap Sci 2003; 29: 382-385.
- [21] Kugge C, Craig VSJ, Daicic J. A scanning electron microscope study of the surface structure of mineral pigments, latices, and thickeners used for paper coating on non-absorbent substrates. Colloids Surfaces A Physicochem Eng Asp 2004; 238: 1-11. <https://doi.org/10.1016/j.colsurfa.2004.02.029>
- [22] Pöhler T, Juvonen K, Sneck A. Coating layer microstructure and location of binder - results from SEM analysis. TAPPI Advanced Coating Fundamentals Symposium 2006; 79-89.
- [23] Lee JH, Lee HL. Characterization of the paper coating structure using focused ion beam and field-emission scanning electron microscopy. 2. structural variation depending on the glass transition temperature of an S/B latex. Ind Eng Chem Res 2018; 57: 16718-16726. <https://doi.org/10.1021/acs.iecr.8b04802>
- [24] Dahlström C, Allem R, Uesaka T. New method for characterizing paper coating structures using argon ion beam milling and field emission scanning electron microscopy. J Microsc 2011; 241: 179-187. <https://doi.org/10.1111/j.1365-2818.2010.03418.x>
- [25] Dahlström C, Uesaka T. Microstructure variations in paper coating: direct observations. Ind Eng Chem Res 2012; 51: 8246-8252. <https://doi.org/10.1021/ie202874z>
- [26] Di Risio S, Yan N. Characterizing coating layer z-directional binder distribution in paper using atomic force microscopy. Colloids Surfaces A Physicochem Eng Asp 2006; 289: 65-74. <https://doi.org/10.1016/j.colsurfa.2006.04.007>
- [27] Patel AA, Feng J, Winnik MA, Vancso GJ, Dittman McBain CB. Characterization of latex blend films by atomic force microscopy. Polymer 1996; 37: 5577-5582. [https://doi.org/10.1016/S0032-3861\(96\)00677-5](https://doi.org/10.1016/S0032-3861(96)00677-5)
- [28] Rajala P, Häkkinen H, Berg CG, Solin R. The effect of intense air drying on material distribution and quality in coated papers. Dry Technol 2003; 21: 1941-1956. <https://doi.org/10.1081/DRT-120026426>
- [29] Hagen KG. Using infrared radiation to dry coatings. Tappi J 1989; 72: 77-83.
- [30] Zang YH, Du J, Du Y, Wu Z, Cheng S, Liu Y. The migration of styrene-butadiene latex during the drying of coating suspensions: When and how does migration of colloidal particles occur? Langmuir 2010; 26: 18331-18339. <https://doi.org/10.1021/la103675f>
- [31] Du Y, Zang YH, Du J. Effects of starch on latex migration and on paper coating properties. Ind Eng Chem Res 2011; 50: 9781-9786. <https://doi.org/10.1021/ie200807w>
- [32] Ranger AE. Binder migration during drying of pigment coatings. Pap Technol 1994; 35: 40-46.
- [33] Jabbal M, Zhong S. The near wall effect of synthetic jets in a boundary layer. Int J Heat Fluid Flow 2008; 29: 119-130. <https://doi.org/10.1016/j.ijheatfluidflow.2007.07.011>
- [34] Lyons A, Iyer R, Bousfield DW. Particle motion modeling for particle size distributions in blade geometries. TAPPI Advanced Coating Fundamentals Symposium 2003; 95-105.
- [35] Pan SX, Davis HT, Scriven LE. Modeling moisture distribution and binder migration in drying paper coatings. Tappi J 1995; 78: 127-143.
- [36] Ferstl E, Gabriel M, Gomernik F, Müller SM, Selinger J, Thaler F, Bauer W, Uhlrig F, Spirk S, Chemelli A. Investigation of the adsorption behavior of jet-cooked cationic starches on pulp fibers. Polym 2020; 12: 2249. <https://doi.org/10.3390/POLYM12102249>
- [37] Wei Q, Zheng H, Zhu M, Han X, Li Y. Starch-based surface-sizing agents in paper industry : An overview. Pap Biomater 2021; 6: 54-61. <https://doi.org/10.1213/j.issn.2096-2355.2021.04.007>
- [38] Sharma M, Aguado R, Murtinho D, Valente AJM, Mendes De Sousa AP, Ferreira PJT. A review on cationic starch and nanocellulose as paper coating components. Int J Biol Macromol 2020; 162: 578-598. <https://doi.org/10.1016/j.ijbiomac.2020.06.131>
- [39] Ghasemian A, Ghaffari M, Ashori A. Strength-enhancing effect of cationic starch on mixed recycled and virgin pulps. Carbohydr Polym 2012; 87: 1269-1274. <https://doi.org/10.1016/j.carbpol.2011.09.010>
- [40] Springer AM, Chandrasekaran S, Wegner TH. Influence of starch on drainage and retention in paperboard mill systems. Tappi J 1984; 67: 104-108.
- [41] Chi K, Wang H, Catchmark JM. Sustainable starch-based barrier coatings for packaging applications. Food Hydrocoll 2020; 103: 105696. <https://doi.org/10.1016/j.foodhyd.2020.105696>
- [42] Scriven LE, Nowicki SC. On the physics of drying and binder migration in coated papers. TAPPI Coating Conference 1990; 49-63.
- [43] Al-Turaif H, Bousfield DW, LePoutre P. The influence of substrate absorbency on coating surface chemistry. Prog Org Coatings 2002; 44: 307-315. [https://doi.org/10.1016/S0300-9440\(02\)00071-1](https://doi.org/10.1016/S0300-9440(02)00071-1)
- [44] Zhen ZH, Wang ZS. Influence of coating binder migration on coated paper optical properties. Adv Mater Res 2013; 746: 114-117. <https://doi.org/10.4028/www.scientific.net/AMR.746.114>
- [45] Zhen ZH, Wang ZS. Study of coating binder migration and affected parameters. adv mater res 2013; 790: 45-48. <https://doi.org/10.4028/www.scientific.net/AMR.790.45>

© 2022 Rao *et al.*; Licensee Lifescience Global.

This is an open access article licensed under the terms of the Creative Commons Attribution License (<http://creativecommons.org/licenses/by/4.0/>) which permits unrestricted use, distribution and reproduction in any medium, provided the work is properly cited.